DNA Melting Investigated by Differential Scanning Calorimetry and Raman Spectroscopy

John G. Duguid,* Victor A. Bloomfield,* James M. Benevides,# and George J. Thomas, Jr.#
* Department of Biochemistry, University of Minnesota, St. Paul, Minnesota 55108 USA, and # Division of Cell Biology and Biophysics, School of Biological Sciences, University of Missouri-Kansas City, Kansas City, Missouri 64110 USA

ABSTRACT Thermal denaturation of the *B* form of double-stranded DNA has been probed by differential scanning calorimetry (DSC) and Raman spectroscopy of 160 base pair (bp) fragments of calf thymus DNA. The DSC results indicate a median melting temperature T_m = 75.5°C with calorimetric enthalpy change ΔH_{cal} = 6.7 kcal/mol (bp), van't Hoff enthalpy change ΔH_{vH} = 50.4 kcal/mol (cooperative unit), and calorimetric entropy change ΔS_{cal} = 19.3 cal/deg · mol (bp), at the experimental conditions of 55 mg DNA/ml in 5 mM sodium cacodylate at pH 6.4. The average cooperative melting unit $\langle n_{melt} \rangle$ comprises 7.5 bp. The Raman signature of 160 bp DNA is highly sensitive to temperature. Analyses of several conformation-sensitive Raman bands indicate the following ranges for thermodynamic parameters of melting: $43 < \Delta H_{vH} < 61$ kcal/mol (cooperative unit), $75 < T_m < 80$°C and $6 < \langle n_{melt} \rangle < 9$ bp, consistent with the DSC results. The changes observed in specific Raman band frequencies and intensities as a function of temperature reveal that thermal denaturation is accompanied by disruption of Watson-Crick base pairs, unstacking of the bases and disordering of the *B* form backbone. These three types of structural change are highly correlated throughout the investigated temperature range of 20 to 93°C. Raman bands diagnostic of purine and pyrimidine unstacking, conformational rearrangements in the deoxyribose-phosphate moieties, and changes in environment of phosphate groups have been identified. Among these, bands at 834 cm^{-1} (due to a localized vibration of the phosphodiester group), 1240 cm^{-1} (thymine ring) and 1668 cm^{-1} (carbonyl groups of dT, dG and dC), are shown by comparison with DSC results to be the most reliable quantitative indicators of DNA melting. Conversely, the intensities of Raman marker bands at 786 cm^{-1} (cytosine ring), 1014 cm^{-1} (deoxyribose ring) and 1092 cm^{-1} (phosphate group) are largely invariant to melting and are proposed as appropriate standards for intensity normalizations.

INTRODUCTION

The strands of double-helical DNA must separate when the genetic information is replicated and transcribed. Thermal denaturation studies of the *B* form of the DNA duplex provide a basis for modeling strand separation. In this paper we use differential scanning calorimetry (DSC) and laser Raman spectroscopy as complementary methods to probe the energetic and structural changes that accompany melting of the *B* form of DNA.

The Raman spectrum of *B* DNA exhibits many bands that are highly sensitive to thermal disordering. Most of the bands in question have been assigned to specific vibrational modes of base and backbone residues. The temperature-dependent changes have been characterized through analyses of the heat treatment of representative mononucleotides, oligonucleotides, polynucleotides, and native nucleic acids (Small and Peticolas, 1971; Lafleur et al., 1972; Thomas and Hartman, 1973; Rimai et al., 1974; Erfurth and Peticolas, 1975). Comprehensive reviews are given by Peticolas et al. (1987), Thomas and Wang (1988), and Thomas and Tsuboi (1993).

Characteristic features of the Raman melting profiles of nucleic acids and their constituents include the following:

1) Raman bands assigned to localized vibrations of the bases undergo increases of intensity as the bases become unstacked and unpaired during melting (Small and Peticolas, 1971; Thomas et al., 1971; Erfurth and Peticolas, 1975; Benevides et al., 1991a; Duguid et al., 1995). This behavior, termed Raman hypochromism, is analogous to the corresponding ultraviolet hypochromism of nucleic acid duplexes and reflects the interdependence of Raman scattering intensity and electronic absorption intensity (Tomlinson and Peticolas, 1970). Relatively large Raman hypochromicities can occur for bands assigned to pyrimidine and purine ring vibrations involving the concerted stretching of conjugated single and double bonds in the heterocycles. These bands generally occur in the regions 600–800 and 1200–1600 cm^{-1} of the Raman spectrum. Examples for *B* DNA are the ring vibrations of adenine near 730 and 1300 cm^{-1}, and of thymine near 750 and 1240 cm^{-1} (Erfurth and Peticolas, 1975; Thomas and Benevides, 1985; Benevides et al., 1991a). A specific Raman hypochromic effect may also be accompanied by a small but detectable shift in the frequency of the band center. For example, the dA marker at 729 cm^{-1} in *B* DNA shifts to 734 cm^{-1} while gaining appreciable intensity upon melting of the native structure.

2) Raman bands of *B* DNA in the interval 800–1100 cm^{-1} are due primarily to vibrational modes of the ordered deoxyribose-phosphate backbone and are highly sensitive in frequency and intensity to DNA melting. The band at 834

Received for publication 31 May 1996 and in revised form 29 August 1996.

Address reprint requests to Dr. George J. Thomas, Jr., Division of Cell Biology and Biophysics, University of Missouri-Kansas City School of Biological Sciences, BSB 405, 5100 Rockhill Rd., Kansas City, MO 64110-2499.

Part LXI in the series Raman Spectral Studies of Nucleic Acids.

0006-3495/96/12/3350/11 $2.00

cm^{-1}, for example, which has been assigned to phosphodiester (OPO) stretching and is diagnostic of the *gauche*$^-$, *gauche*$^-$ geometry of phosphodiester groups of *B* DNA (Erfurth and Peticolas, 1975; Benevides et al., 1988; Tajmir-Riahi et al., 1988), is diminished in intensity in direct proportion to the elimination of *B* DNA structure with increasing temperature (Benevides et al., 1991a). In single stranded DNA at elevated temperatures, the 834 cm^{-1} marker is not discernible and is replaced by a very broad and weak distribution of Raman intensity extending from ~800 to 850 cm^{-1} (Benevides et al., 1991a). Similar intensity decreases and broadening are observed for *B* DNA marker bands near 895 and 920 cm^{-1}, also assigned to backbone vibrations. The temperature dependency of these bands again reflects conformational heterogeneity in the phosphodiester backbone of denatured DNA. In the case of RNA, as well as the *A* form of DNA, analogous markers of backbone geometry have been identified in the spectral interval 800–1100 cm^{-1}, and their conformational dependence has been reported (Thomas et al., 1971; Lafleur et al., 1972; Thomas and Hartman, 1973).

3) All native nucleic acids exhibit a broad and intense band near 1668 cm^{-1}, which originates from coupled C═O stretching and N—H deformation modes of base exocyclic groups, with carbonyls of dT (or rU) being the greatest contributor. The composite band is highly sensitive to disruption of Watson-Crick hydrogen bonding (Lafleur et al., 1972; Morikawa et al., 1973; Erfurth and Peticolas, 1975; Benevides et al., 1991a). For example, thermal denaturation of *B* DNA leads to a large increase of the band intensity and a pronounced shift of the band center to lower frequency. This behavior probably reflects different contributions of the thymine carbonyl acceptors when hydrogen bonded to adenine or water molecules. Corresponding changes occur upon thermal denaturation of RNA, attributable to the altered hydrogen bonding of uracil (Lafleur et al., 1972).

The effect of temperature upon the nucleic acid duplex may also be investigated by DSC, which measures the heat absorbed during thermal denaturation and provides an experimental basis for determining thermodynamic parameters that govern the melting transition (Breslauer et al., 1986; Breslauer et al., 1992). By monitoring the progress of the transition, DSC also enables a definitive determination that the process has gone to completion. The DSC measurement provides the median melting temperature of the transition, T_m, and the associated changes in the calorimetric enthalpy, ΔH_{cal}, and entropy, ΔS_{cal}. With further manipulation of the DSC data, the van't Hoff enthalpy, ΔH_{vH}, and the effective number of base pairs, $\langle n_{melt} \rangle$, in a cooperative melting unit can be determined. By fitting the DSC melting curve to that predicted from helix-coil transition theory, it is also possible to extract the apparent helix nucleation parameter, σ, which constitutes a measure of melting cooperativity (Cantor and Schimmel, 1980).

In this study we have combined Raman spectroscopy with DSC to characterize the thermal melting of 160 bp fragments of calf thymus DNA. We have identified Raman bands of *B* DNA representing each of the three categories delineated above and have focused on a quantitative analysis of their temperature dependencies. Melting behaviors of the separate Raman markers have been correlated with one another over the temperature interval 11–93°C. The results have been interpreted structurally and discussed in connection with previous observations, revealing previously undetected features of the temperature-dependent Raman spectrum of DNA. From the DSC results, we have obtained the standard thermodynamic parameters noted above and correlated them with the localized structural changes monitored by Raman spectroscopy.

We have analyzed in detail the temperature dependence of Raman bands at 834, 1240, and 1668 cm^{-1} to obtain independent estimates of T_m and ΔH_{vH}. The values determined by Raman spectroscopy agree well with those obtained by DSC, showing that detailed spectroscopic measurements of backbone and base perturbations are consistent with the overall thermodynamic changes that occur during thermal melting of *B* DNA.

MATERIALS AND METHODS

Preparation of DNA

Mononucleosomal calf thymus DNA (160 ± 5 bp) was prepared using standard methods (Strzelecka and Rill, 1987; Wang et al., 1990) and purified by three successive phenol extractions. One and one-half volumes of cold isopropanol (−20°C) were added to the aqueous DNA-containing layer and the mixture was stored overnight at −20°C. The precipitated DNA was removed by centrifugation at 8000 rpm in a Beckman JA-10 rotor for 45 min, dried, and resuspended in 10 mM Na_2HPO4 + 0.2 M NaCl + 1 mM Na_2EDTA (pH 7.5). The solution was dialyzed twice against 4 M NaCl + 5 mM EDTA (pH 7.5), twice against 1 M NaCl (pH 7.5), and four times against Milli-Q water, then lyophilized. The lyophilizate was desiccated at −20°C. An aqueous solution of DNA (5% w/w) was prepared in 5 mM sodium cacodylate at pH 6.5 and maintained at 4°C prior to spectroscopic and calorimetric measurements.

Differential scanning calorimetry

DNA and reference solutions were saturated with helium for 30 min before data acquisition to reduce bubble formation upon heating. DNA and reference buffer, each 1.5 ml in volume, were loaded into their respective reservoirs in a MicroCal MC-2 Differential Scanning Calorimeter (Amherst, MA). An external pressure of 40 psi was applied to both the sample and reference cell. Temperature regulation was achieved with a computer-controlled Haake F3-CH circulator. The sample was scanned relative to the reference buffer over the temperature range 10–98°C at a rate of 12 K/h^{-1}. Data were obtained using the DA-2 acquisition system (MicroCal) under the control of an IBM microcomputer interfaced to the calorimeter through a Data Translation AT 2801 IO board (Marlboro, NH). Heat capacity (ΔC_p) plots were cell and baseline-corrected according to standard techniques (Hinz, 1986; Sturtevant, 1987). The calorimetric enthalpy (ΔH_{cal}) and entropy (ΔS_{cal}) changes were obtained as areas under plots versus temperature of ΔC_p and $\Delta C_p/T$, respectively. The melting temperature, T_m, was determined from the equilibrium condition

$$T_m = \Delta H_{cal}/\Delta S_{cal}. \quad (1)$$

The van't Hoff enthalpy, ΔH_{vH}, was obtained from the relation

$$\Delta H_{vH} = 6RT_m^2[\Delta C_p(T_m)/\Delta H_{cal}] \quad (2)$$

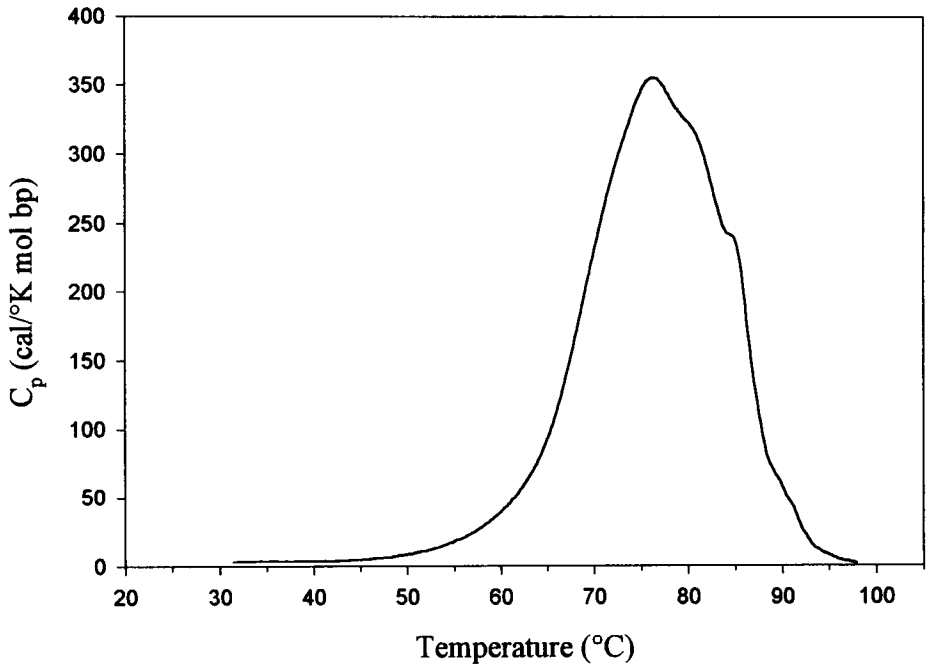

FIGURE 1 DSC heat capacity curve of 160-bp fragments of calf thymus DNA dissolved to 55 mg/ml in 5 mM sodium cacodylate, pH 6.4.

where R is the gas constant and $\Delta C_p(T_m)$ is the difference in molar heat capacity between helical (duplex) and coil (heat denatured) forms at the melting temperature. The average number of base pairs, $\langle n_{melt} \rangle$, in a cooperative melting unit was calculated from the ratio

$$\langle n_{melt} \rangle = \Delta H_{vH}/\Delta H_{cal}. \quad (3)$$

We evaluated the apparent helix initiation parameter (σ) using helix-coil transition theory (Cantor and Schimmel, 1980). The equilibrium constant for helix propagation, s, is determined as a function of T from the expression

$$\ln(s) = (\Delta H_{cal}/R)(1/T - 1/T_m). \quad (4)$$

From helix-coil transition theory for short chains, the fractional extent of melting is

$$\theta = (s/2\lambda)\{1 + [s - 1 + 2\sigma]/[(1 - s)^2 + 4\sigma s]^{1/2}\} \quad (5)$$

where

$$\lambda = \frac{1}{2}\{(1 + s) + [(1 - s)^2 + 4\sigma s]^{1/2}\}. \quad (6)$$

We determined the experimental coil fraction, θ_{exp}, by integrating the heat capacity curve and normalizing the resulting integral to unity. After substituting values of θ_{exp} and s into Eqs. 5 and 6, we adjusted σ until the best fit was obtained. Subsequent substitution of σ into Eq. 5 allowed calculation of θ for comparison with experimental measurements.

Raman difference spectroscopy

Aliquots of DNA solution (≈10 μl) were sealed in glass capillaries (Kimax No. 34502) for Raman analysis. Spectra were excited with the 514.5 nm line of an Innova 70 argon laser (Coherent, Santa Clara, CA) using approximately 200 mW of radiant power at the sample, and were collected on a Model 1877 triple spectrograph (Spex Instruments, Metuchen, NJ) equipped with an OMA-III intensified diode array detector (Princeton Applied Research, Princeton, NJ). Data were obtained at 5°C increments over the temperature range 11–93°C on samples thermostated to within ±0.5°C of the specified temperature. Signal-to-noise ratios were improved by accumulating and averaging up to several hundred exposures of 1 min each in the spectral interval 600–1750 cm^{-1}. Weak background scattering by the aqueous solvent was removed using computer subtraction techniques described previously (Prescott et al., 1984; Duguid et al., 1993).

Difference spectra were computed using the convention of Langlais et al. (1990): difference spectrum = spectrum of DNA at temperature T minus the spectrum of DNA at 20°C. For normalization of Raman intensities in the minuend and subtrahend, we used either the intense band at 786 cm^{-1} or the weaker band near 1014 cm^{-1}, the intensities of which have been shown previously (and confirmed here) to be independent of temperature (Erfurth and Peticolas, 1975; Benevides et al., 1991a). Each Raman

TABLE 1 Thermodynamic parameters for the melting of 160 bp calf thymus DNA

Method	ΔH_{cal} [kcal/mol(bp)]	ΔH_{VH} [kcal/mol]	ΔS_{cal} [cal/deg · mol(bp)]	T_m (°C)	$\langle n_{melt} \rangle$ (bp)	σ ($\times 10^3$)
DSC	6.7	50.4	19.3	75.5	7.5	10.9
Raman (cm^{-1})						
834	—	43.4	—	75.3	6.5	—
1240	—	47.1	—	79.2	7.0	—
1668	—	60.4	—	75.5	9.0	—
Average	—	50.3	—	76.7	7.5	—

intensity is reported as the peak height at the band maximum measured above a baseline tangent to the wings of the band.

Experimental errors associated with Raman intensity measurements were evaluated as described previously (Duguid et al., 1993). In accord with the additivity of variances, the root-mean-square deviation in Raman band intensity at frequency ν, δI_ν, is given by the relation

$$\delta I_\nu = (\delta I_{bl}^2 + \delta I_{1014}^2)^{1/2} \quad (7)$$

where δI_{bl} and δI_{1014} are, respectively, the root-mean-square deviations (noise levels) in the spectral baseline and reference band at 1014 cm^{-1}. The margin of error, which is given by $5.0 \times \delta I_\nu$, represents 99.7% confidence that the measured band intensity is within $\pm 2.5(\delta I_\nu)$.

Van't Hoff enthalpies of DNA melting were calculated from the temperature dependencies of the Raman intensities at 834, 1240, and 1668 cm^{-1}, each normalized between 0 and 1 to give the fractional helicity θ as a function of T. The value of T_m was determined from each band as the temperature at which the respective θ value (θ_{834}, θ_{1240} and θ_{1668}) achieved 50% of its maximal change. The slope of the plot of θ versus T in the vicinity of T_m was used to compute ΔH_{vH} according to the equation

$$\Delta H_{vH} = 6RT_m^2(\partial\theta/\partial T)_{T=T_m}. \quad (8)$$

RESULTS

Differential scanning calorimetry

The DSC curve for melting of 160 bp fragments of calf thymus DNA is shown in Figure 1. As expected, the melting transition is broad owing to the heterogeneous base composition of the calf thymus DNA fragments and the low ionic strength (5 mM sodium cacodylate) employed in these experiments.

The thermodynamic parameters derived from Figure 1 are given in Table 1. The values of ΔH_{cal} and ΔS_{cal} are consistent with previous results (Breslauer et al., 1986). The ratio $\Delta H_{vH}/\Delta H_{cal}$ signifies an average cooperative melting unit of 7.5 bp which, however, is significantly smaller than values obtained for other types of DNA. A similar difference occurs in the value of $\sigma = 1.09 \times 10^{-2}$, obtained by fitting the integrated and normalized transition curve of Figure 2 using helix-coil transition theory. The present value of σ is roughly two orders of magnitude greater than values determined previously for a variety of synthetic polynucleotides (Crothers et al., 1964; Gruenwedel, 1975; Oliver et al., 1977) and high-molecular-weight viral DNA (Wada et al., 1980). This difference may reflect differences in base composition and sequence of the various DNAs.

Raman spectroscopy

Figure 3 shows the Raman spectrum of 160 bp fragments of calf thymus DNA at 20°C (*top trace*), and compares difference spectra computed between 20°C (subtrahend) and several higher temperatures (24, 29, 38, 46, 55, 64, 72, 77, 81, 86 and 93°C, each as minuend). Figure 4 displays melting profiles of the more prominent Raman bands, plotted as band intensity I_ν versus temperature, where I_ν is the peak height of the Raman band at frequency ν. The Raman profiles of Figure 4 are believed to reflect primarily the following structural changes as a function of increasing temperature: I_{834}, decreasing population of ordered (*B* form) phosphodiester groups; I_{729}, and I_{1305}, unstacking of d*A*; I_{1187}, unstacking of dT and dC; I_{1240}, unstacking of d*T*; I_{1668}, rupture of hydrogen bonds between dA · dT and dG · dC base pairs; I_{1338}, unstacking of d*G* and d*A*; I_{1375}, unstacking of dT, dA, and dG; I_{1421}, alteration of deoxyribose conformation. The basis for band assignments and structural correlations has been discussed elsewhere (Bene

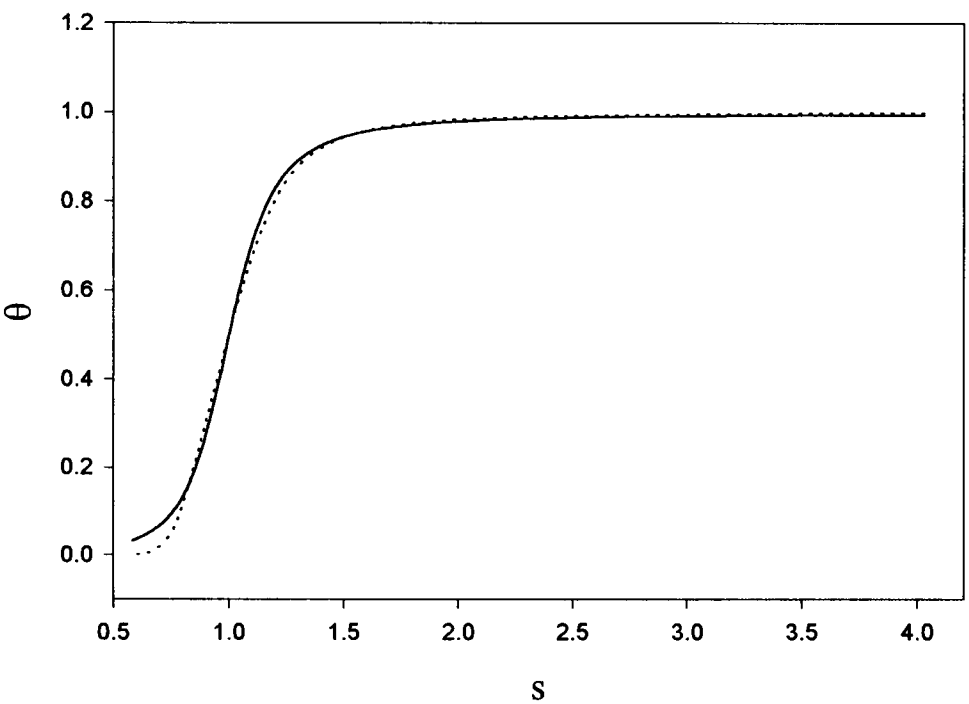

FIGURE 2 Comparison of experimental (*dotted line*) and calculated values (*solid line*) of the fractional helicity, θ, as a function of the equilibrium constant for helix propagation, S. The calculated curve is based upon $\sigma = 1.09 \times 10^{-2}$, the optimized value (best fit to experimental data) for the helix initiation parameter.

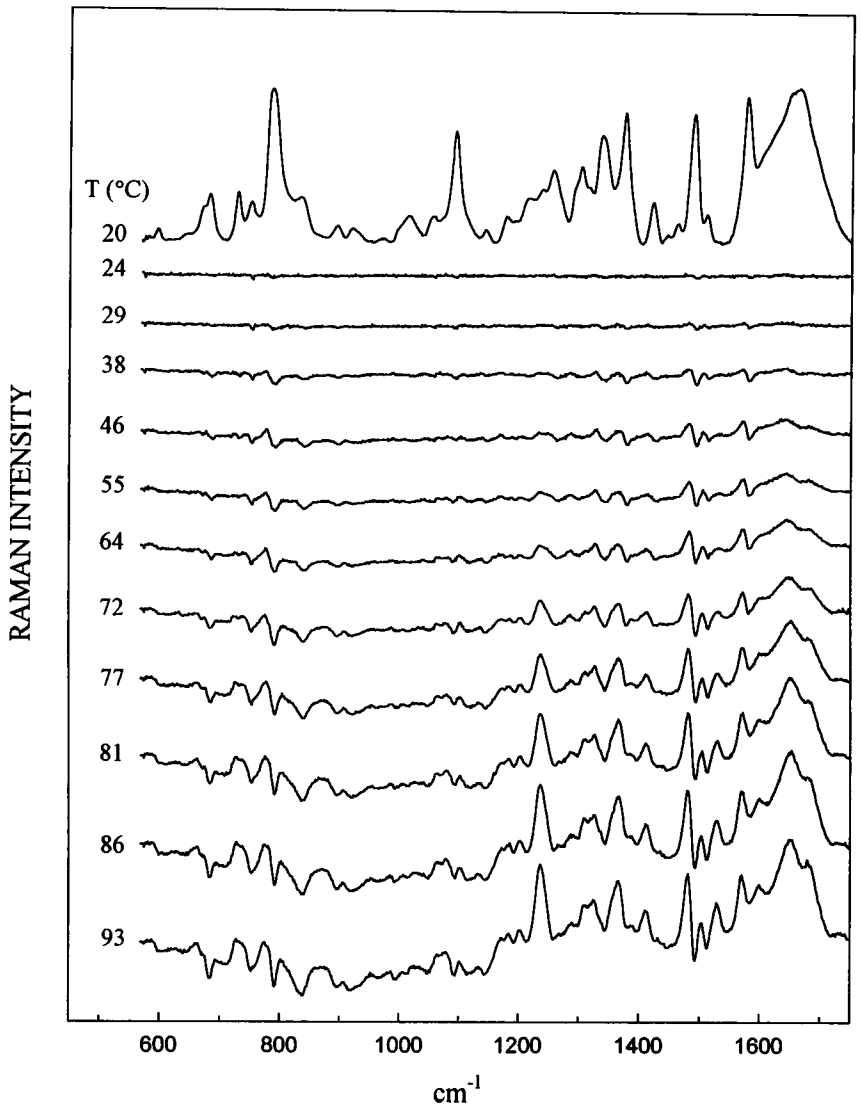

FIGURE 3 Raman spectrum of 160-bp fragments of calf thymus DNA at 55 mg/ml in 5 mM sodium cacodylate (pH 6.4) and 20°C (*top trace*). Lower traces are difference spectra obtained by subtracting the spectrum measured at the indicated temperature from the spectrum measured at 20°C. Difference intensities reflect the actual change in intensity of the parent band in the 20°C spectrum.

vides et al., 1988; Thomas et al., 1995; Thomas and Tsuboi, 1993).

The d*G* marker at 681 cm^{-1} exhibits notable behavior. As temperature increases, the peak height (I_{681}) exhibits a relatively small though significant decrease, mainly between 60 and 90°C (Figure 4), with a concomitant shift of the band center to lower frequency (Figure 3). This behavior is considered to represent the composite of several effects, which may be understood as follows. The 681 cm^{-1} frequency is a definitive marker of the C2′-*endo/anti* dG conformation and is diagnostic of *B* form DNA (Benevides et al., 1988). Markers of other dG conformers occur just below 680 cm^{-1}, including the C3′-*endo/anti* conformer at 664 cm^{-1} and related conformers between 660 and 680 cm^{-1} (Thomas and Wang, 1988). Thus, as the *B* form structure is melted and the population of dG conformers changes from predominantly C2′-*endo/anti* to a mixture of many different conformers, the intensity decreases at 681 cm^{-1} but increases at slightly lower frequencies (660–680 cm^{-1}) (data not shown). The latter intensity increases partially compensate the former decrease because the bands overlap so extensively. The net effect is only a small change in the intensity at 681 cm^{-1} and a shift of the apparent band center to lower frequency.

Numerous other bands in the DNA spectrum of Figure 3 also exhibit sensitivity to temperature. For example, the thymidine band near 750 cm^{-1}, which identifies C2′-*endo/anti* conformers of dT (Thomas and Benevides, 1985), also broadens and shifts to lower frequency (≈738 cm^{-1}) in a manner similar to that observed for the dG marker at 681 cm^{-1}. As in the case of dG, the shift of the C2′-*endo/anti* dT marker to lower frequency is partially obscured by overlapping bands which increase in intensity. Nevertheless, the trend can be discerned in the difference spectra of Figure 3. The data are consistent with the conversion of dT and dG, and presumably also dC and dA, from exclusively C2′-*endo/anti* conformations at 20°C to a broad distribution of nucleoside conformations at high temperature.

Like the dG marker at 681 cm^{-1}, the phosphodiester marker at 834 cm^{-1} also decreases in intensity as DNA

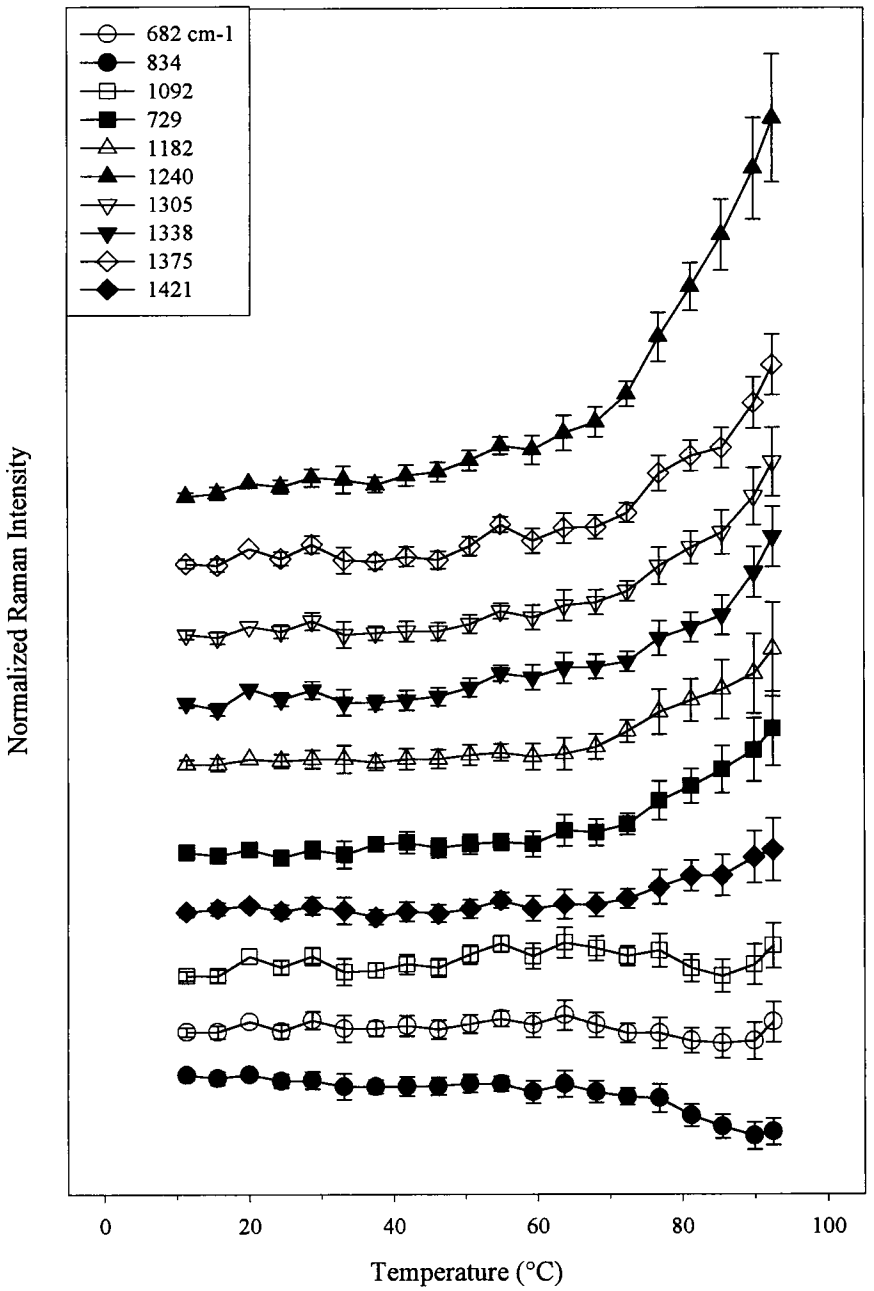

FIGURE 4 Melting profiles of representative Raman bands of 160-bp calf thymus DNA. Intensity changes of all bands are normalized to the same scale. Error bars indicate uncertainties in the measured intensities, estimated with Eq. 7. Uncertainties are omitted for data points at the reference temperature (20°C), and below 30°C are smaller than the data point symbols. Specific band assignments and additional details are given in the text.

undergoes thermal denaturation. This intensity decrease, shown in Figure 4, correlates well with the heat capacity curve for DNA melting (Figure 1) and is attributed to an increase in conformational flexibility of the DNA backbone. Similar intensity decreases are also observed for the bands at 895 and 923 cm^{-1}, which are assigned to the DNA backbone.

The band at 1092 cm^{-1}, assigned to the symmetric phosphodioxy (PO_2^-) stretching vibration, is seen in Figure 4 to exhibit little net change in intensity between 10 and 90°C, although small fluctuations in the peak height are apparent throughout the temperature interval. In model diester phosphates, the corresponding Raman band is sensitive to interactions of metal ions and solvent molecules with the PO_2^- groups (Aubrey et al., 1992; Stangret and Savoie, 1992). Here, we observe some evidence of band broadening with temperature, mainly between 75 and 90°C, which can be attributed to changes in PO_2^- environments upon melting of the double helix. Nevertheless, the peak intensity overall is largely independent of temperature and the 1092 cm^{-1} band should be reliable as an internal intensity standard.

Negative difference bands of weak-to-moderate intensity appear near 805 and 872 cm^{-1} in the Figure 3 difference spectra. While definitive assignments are not yet possible, intensity changes of similar frequency and intensity are observed in spectra of thermally denatured oligonucleotides (Benevides et al., 1991a) and acid denatured calf thymus DNA (Puppels et al., 1994). A similar band at 872 cm^{-1}

accompanies the *B*-to-*C* structure transformation of calf thymus DNA fibers (Erfurth et al., 1972), driven by lowering the relative humidity of the sample. Disruption of hydrogen bonding between water molecules and polar groups of the sugar-phosphate backbone, as a consequence of either elevating the solution temperature, lowering the solution pH, or lowering the relative humidity in fibers, may produce the band at 872 cm^{-1}.

Hypochromic Raman bands of the DNA bases exhibit pronounced intensity increases with thermal denaturation. Several are shown in Figure 4. In each case, the intensity recovery is attributed largely to base unstacking (Erfurth and Peticolas, 1975; Benevides et al., 1991a). Typically, the intensity increases gradually between 60 and 80°C, attenuates somewhat between 80 and 85°C, then resumes increasing intensity above 85°C. In each case, the latter increase persists to the highest temperature monitored (93°C). In addition to these intensity changes, the Raman bands of this spectral interval exhibit shifts to lower frequency, possibly reflecting the altered hydrogen bonding states of the base residues.

Of particular interest is the Raman band near 1489 cm^{-1}, assigned mainly to the guanine ring. The band is sensitive to interactions of electrophiles with the N7 acceptor (Nishimura et al., 1986, Benevides et al., 1991b, 1991c). Figure 3 shows that the 1489 cm^{-1} band shifts to lower frequency with thermal denaturation, an effect which can be attributed to stronger hydrogen bonding of solvent with the guanine N7 site in denatured DNA. The 1489 cm^{-1} band also shows a dramatic increase in intensity as DNA melting nears completion. Similar behavior is observed for the purine band at 1578 cm^{-1}. These effects may be attributed to the recovery of Raman intensity (elimination of hypochromism) with denaturation. Evidently, purine unstacking is the last local structural change to take place with melting.

The broad band centered near 1668 cm^{-1} contains contributions from coupled C=O stretching and NH deformation modes of dT, dG, and dC, with dT as the major contributor. Figure 3 shows that DNA melting leads to diminished intensity at 1668 cm^{-1} and enhanced intensity at lower (1658 cm^{-1}) and higher (1684 cm^{-1}) frequencies. These results are consistent with earlier findings on model DNA (Erfurth et al., 1972) and RNA structures (Lafleur et al., 1972; Small and Peticolas, 1971). By analogy with the model compound studies, the two bands of denatured DNA are assigned to modes involving primarily C4=O and C2=O stretching of dT.

Table 2 is a matrix of correlation coefficients relating the temperature-induced intensity changes of specific Raman bands with one another. The tabulation shows that, except for the bands at 1092 (PO_2^- symmetric stretching) and 681 cm^{-1} (dG), the temperature-dependent intensities of DNA Raman bands are all strongly correlated with one another, which implies concerted behavior of the corresponding moieties during thermal denaturation. The absence of significant intensity change at 1092 cm^{-1} is consistent with the assignment to the highly localized PO_2^- group vibration. On the other hand, the exceptional behavior of the dG marker at 681 cm^{-1} is believed to reflect the depopulation of C2′-*endo/anti* conformers and competing effects of the temperature-sensitive dT marker with which it is overlapped. Representative correlations for the 834 cm^{-1} backbone marker and 1305 cm^{-1} dA marker, are illustrated graphically in Figure 5.

Estimation of thermodynamic parameters using Raman intensities

The intensities of several Raman bands vary monotonically with temperature through the melting region in such a way as to suggest that they can be employed as quantitative measures of helix denaturation. This is shown in Figure 6, *A* and *B*, where the normalized intensities of the 834, 1240 and 1668 cm^{-1} bands are compared with ΔH (proportional to fractional melting) determined by DSC. The melting temperatures and van't Hoff enthalpies obtained from these Raman bands are compared with the DSC values in Table 1. The agreement is reasonably good, showing the suitability of the selected Raman band intensities for providing ther

TABLE 2 Correlation coefficients relating temperature-dependent intensities of DNA Raman bands

cm^{-1}	681	729	750	834	1092	1187	1240	1305	1338	1375	1421	1489	1578	1668
681	—	0.18	0.08	0.30	0.46	0.31	0.19	0.14	0.09	0.13	0.16	0.04	0.06	0.14
729			0.87	0.93	0.02	0.98	0.99	0.99	0.97	0.98	0.95	0.91	0.91	0.96
750				0.74	0.01	0.09	0.86	0.88	0.87	0.87	0.88	0.76	0.73	0.76
834					0.01	0.92	0.94	0.90	0.87	0.89	0.87	0.82	0.83	0.89
1092						0.02	0.02	0.04	0.08	0.05	0.03	0.17	0.16	0.07
1187							0.99	0.99	0.96	0.98	0.97	0.90	0.90	0.96
1240								0.99	0.97	0.98	0.97	0.92	0.92	0.97
1305									0.99	0.99	0.98	0.94	0.94	0.97
1338										0.99	0.96	0.96	0.96	0.97
1375											0.98	0.95	0.95	0.97
1421												0.90	0.89	0.94
1489													0.99	0.96
1578														0.98
1668														—

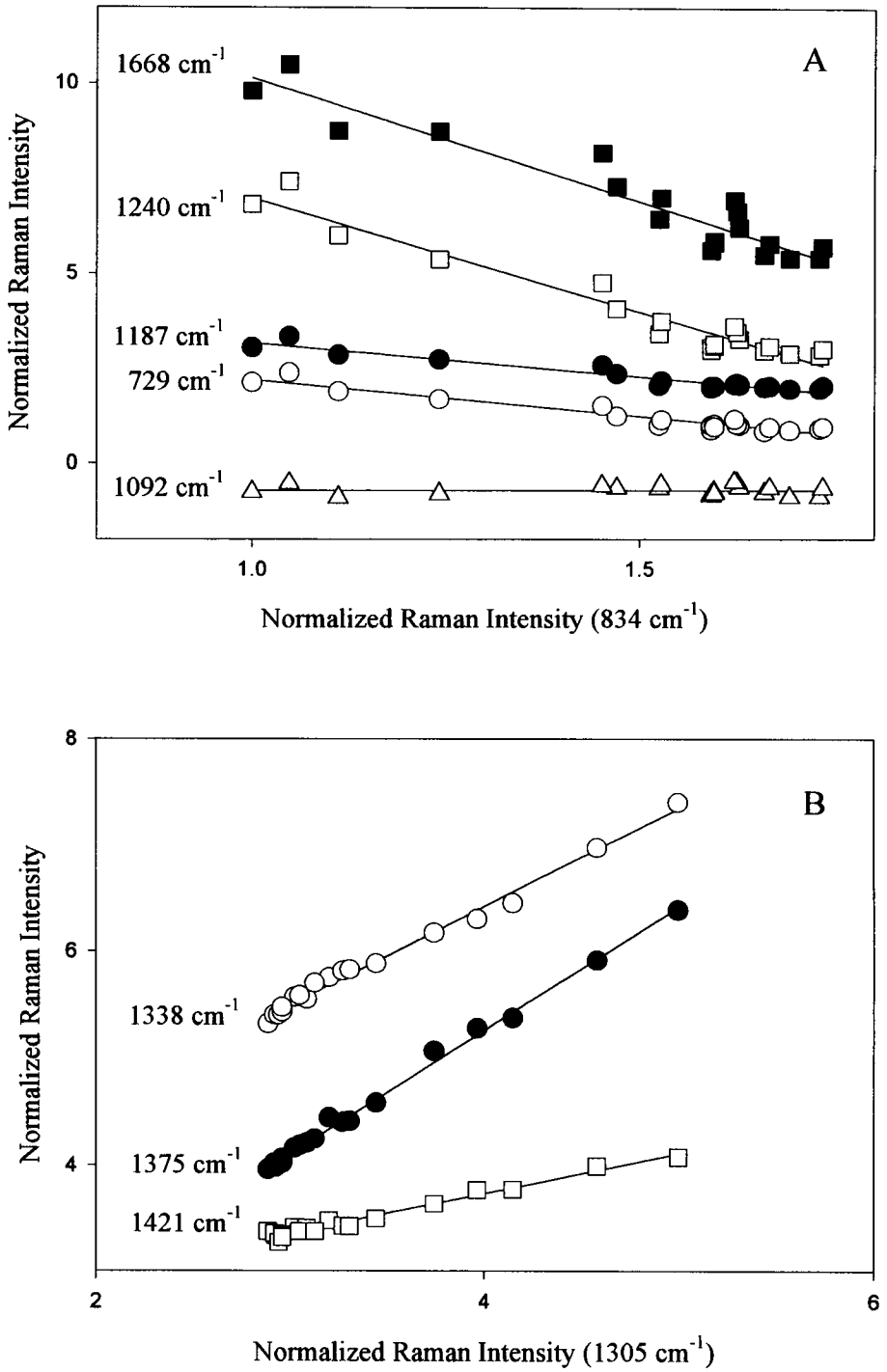

FIGURE 5 Panel (*A*): Correlation of the temperature dependence (20–93°C) of the *B* form backbone marker at 834 cm^{-1} with the temperature dependencies of the following purine and pyrimidine markers: 729 cm^{-1} (dA) (○); 1187 cm^{-1} (dT and dC) (●); 1240 cm^{-1} (dT) (□); 1668 cm^{-1} (carbonyls) (■). Respective correlation coefficients are 0.93, 0.92, 0.94, and 0.89 (data from Table 2). Also shown is the intensity of the 1092 cm^{-1} band, which is not temperature dependent. Panel (*B*): Correlation of the temperature dependence (20–93°C) of the adenine marker at 1305 cm^{-1} with the temperature dependencies of the following markers: 1338 cm^{-1} (dG, dA) (○); 1375 cm^{-1} (dT, dA, dG), (●); 1421 cm^{-1} (deoxyribose). (□). Respective correlation coefficients are 0.99, 0.99, 0.98 (data from Table 2).

modynamic parameters as well as structural information related to DNA melting.

DISCUSSION

Table 3 summarizes the perturbations to Raman intensities and frequencies that result from the thermal denaturation of 160-bp fragments of calf thymus DNA. The results obtained in this Raman study are qualitatively similar in many respects to those obtained previously on high-molecular-weight calf thymus DNA (Erfurth and Peticolas, 1975). However, the present use of multichannel Raman instrumentation in combination with digital difference methods has permitted for the first time a quantitative thermodynamic analysis of DNA melting on the basis of Raman spectral perturbations. Appropriate for thermodynamic characterization of DNA melting are Raman bands that exhibit monotonic intensity changes with temperature, typ

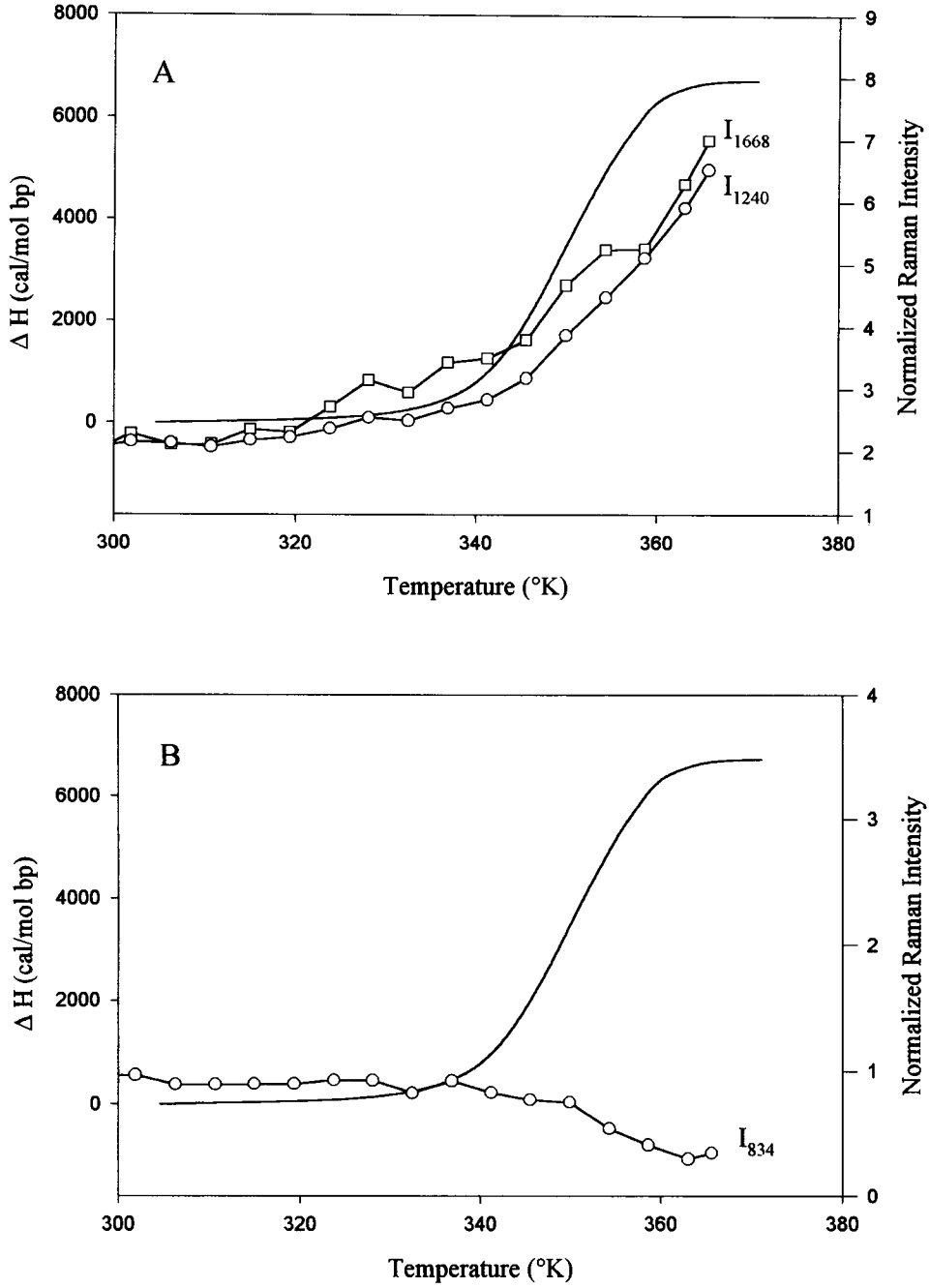

FIGURE 6 (*A*) Comparison of ΔH measured by DSC (*solid line, left ordinate*) with Raman intensities (*right ordinate*) at 1240 cm^{-1} (○) and 1668 cm^{-1} (□). (*B*) Comparison of ΔH measured by DSC (*solid line, left ordinate*) with the Raman intensity (*right ordinate*) at 834 cm^{-1} (○).

ified by the bands at 834, 1240, and 1668 cm^{-1} (Fig. 6). Comparison of the Raman melting results with those obtained by DSC measurements on identical DNA samples (Table 1) indicates that reliable estimates of thermodynamic parameters (ΔH_{vH}, T_m, $\langle n_{melt} \rangle$) are obtained from the Raman analysis.

The present Raman spectra reveal further that intensity versus temperature profiles for many key Raman bands of the DNA bases are more complex than previously suggested. Several marker bands exhibit nonmonotonic intensity dependence upon temperature, implying either that the bands in question monitor more than one type of local structural change with temperature or that the changes being monitored are not linearly dependent upon temperature. This type of behavior is exemplified by several bands of the 1150–1450 cm^{-1} interval (Fig. 4), each of which exhibits an attenuation of intensity increase near 80°C followed by a continued intensity increase. The results may reflect different stacking arrangements at different stages of the melting transition, a concept consistent with the observed frequency shifts in the Raman bands. The significance of such frequency shifts in the case of base-ligand interactions has been discussed in detail in a recent study of metal-induced DNA melting (Duguid et al., 1995).

TABLE 3 Raman spectral changes accompanying the melting of DNA

Parent band (cm^{-1})	Assignment[a]	Perturbed Raman band[b] (cm^{-1})
729	dA	+725w
750	dT	+738w
781	dC	+773, −792s
805	bk	+803m
895	bk	+872vw
1054	bk(νCO)	+1060w
1187	dT, dC	+1183w
1218	dT	
1240	dT	+1240s
1258	dC, dA	
1292	dC	+1289m
1303	dA	+1308m
1320	dG	
1335	dA, dG	+1324, −1343m
1374	dT, dA, dG	+1363, −1381s
1421	δCH_2, dA	+1412m
1489	dG, dA	+1481, −1494s
1512	dA	+1504vw
1532	dC	+1528m
1578	dG, dA	+1572, −1582m
1602	dC	+1597vw
1688	$\nu C{=}O$, δNH_2 dT, dG, dC	+1654m, +1684m

[a]Bands assigned to nucleosides are indicated by dG, dA, dT, dC. Other abbreviations: bk, backbone; νOPO, phosphodiester stretching mode; νCO, sugar C—O stretching mode; νPO_2^-, phosphodioxy stretching mode; δCH_2, methylene deformation mode; $\nu C{=}O$, carbonyl stretching mode; δNH_2, amino scissoring mode.

[b]Frequency (cm^{-1}) and relative intensity (vw, very weak; w, weak; m, medium; s, strong; vs, very strong; sh, shoulder) of the perturbed Raman band in the 93°C spectrum. Plus (or minus) sign indicates a difference peak (or trough), signifying that the parent band has gained (or lost) appreciable intensity as a result of DNA melting between 20 and 93°C.

In accordance with other investigations (Erfurth and Peticolas, 1975; Duguid et al., 1993, 1995), we have found that the intensities of Raman bands at 786 and 1014 cm^{-1} are not affected significantly by temperature changes. The invariance of these band intensities is also confirmed by melting profiles obtained on protein-nucleic acid and salt-nucleic acid mixtures (reviewed in Thomas and Tsuboi, 1993). Additionally, the present results indicate that the peak intensity of the band at 1092 cm^{-1}, a marker of the PO_2^- group, is not highly sensitive to DNA melting at the conditions of the present experiments. Model compound studies (Aubrey et al., 1992; Stangret and Savoie, 1992) show, however, that the band is affected by high local concentrations of divalent cations. Accordingly, the 1092 cm^{-1} band is appropriate for intensity standardization in Raman spectra of DNA at conditions comparable to those of present measurements (i.e., low concentrations of NaCl), but not generally for solutions that may contain high concentrations of divalent cations.

In a previous paper of this series (Duguid et al., 1993), we demonstrated the usefulness of correlating the spectral perturbations of specific Raman bands with one another. Such tabular correlations facilitate identification of coupled structural changes involving different DNA moieties. In this work, we have shown that strong correlations exist between temperature-induced changes in nucleoside furanose pucker, backbone order, thymine base stacking, A · T and G · C base pairing, and phosphate group interactions of DNA (Table 2). Additionally, bands in the interval 1150–1450 cm^{-1}, due primarily to purine ring vibrations, constitute a second group of bands that are strongly correlated with one another, though not correlated with the first group of bands. The latter reflect more complex structural changes with temperature, which will be addressed in future studies.

J. Duguid was the recipient of a Molecular Biophysics Predoctoral Traineeship from NIH (GM08277) and acknowledges the assistance of R. Becka and K. Reilly (UMKC) during various stages of this work.

This research was supported by NIH Grants GM28093 (V.A.B.) and GM54378 (G.J.T.).

REFERENCES

Aubrey, K. L., S. R. Casjens, and G. J. Thomas, Jr. 1992. Secondary structure and interactions of the packaged dsDNA genome of bacteriophage P22 investigated by Raman difference spectroscopy. *Biochemistry.* 31:11835–11842.

Benevides, J. M., A. H.-J. Wang, G. A. van der Marel, J. H. van Boom, and G. J. Thomas, Jr. 1988. Crystal and solution structures of the *B* DNA dodecamer d(CGCAAATTTGCG) probed by Raman spectroscopy: heterogeneity in the crystal structure does not persist in the solution structure. *Biochemistry.* 27:931–938.

Benevides, J. M., P. L. Stow, L. L. Ilag, N. L. Incardona, and G. J. Thomas, Jr. 1991a. Differences in secondary structure between packaged and unpackaged single-stranded DNA of bacteriophage ϕX174 determined by Raman spectroscopy: a model for ϕX174 DNA packaging. *Biochemistry.* 30:4855–4863.

Benevides, J. M., M. A. Weiss, and G. J. Thomas, Jr. 1991b. Design of the Helix-turn-helix motif: nonlocal effects of quaternary structure in DNA recognition investigated by laser Raman spectroscopy. *Biochemistry.* 30:4381–4388.

Benevides, J. M., M. A. Weiss, and G. J. Thomas, Jr. 1991c. DNA recognition by the helix-turn-helix motif: investigation by laser Raman spectroscopy of the phage λ repressor and its interaction with operator sites O_L1 and O_R3. *Biochemistry.* 30:5955–5963.

Breslauer, K. J., R. Frank, H. Blocker, and L. A. Markey. 1986. Predicting DNA duplex stability from the base sequence. *Proc. Natl. Acad. Sci. U.S.A.* 83:3746–3750.

Breslauer, K. J., E. Freire, and M. Straume. 1992. Calorimetry: a tool for DNA and ligand-DNA studies. *Methods Enzymol.* 211:533–567.

Cantor, C. R., and P. R. Schimmel. 1980. Biophysical Chemistry. III. The Behavior of Biological Macromolecules. W. H. Freeman & Co., San Francisco.

Crothers, D. M., N. R. Kallenbach, and B. H. Zimm. 1964. Theory of the melting transition of synthetic polynucleotides: evaluation of the stacking free energy. *J. Mol. Biol.* 9:1–9.

Duguid, J., V. A. Bloomfield, J. M. Benevides, and G. J. Thomas, Jr. 1993. Raman spectroscopy of DNA-metal complexes. I. Interactions and conformational effects of the divalent cations: Mg, Ca, Sr, Ba, Mn, Co, Ni, Cu, Pd, and Cd. *Biophys. J.* 65:1916–1928.

Duguid, J. G., V. A. Bloomfield, J. M. Benevides, and G. J. Thomas, Jr. 1995. Raman spectroscopy of DNA-metal complexes. II. Thermal denaturation of DNA in the presence of Sr^{2+}, Ba^{2+}, Mg^{2+}, Ca^{2+}, Mn^{2+}, Co^{2+}, Ni^{2+}, and Cd^{2+}. *Biophys. J.* 69:2623–2641.

Erfurth, S. C., E. J. Kiser, and W. L. Peticolas. 1972. Determination of the backbone structure of nucleic acid oligomers by laser Raman scattering. *Proc. Natl. Acad. Sci. U.S.A.* 69:938–941.

Erfurth, S. C., and W. L. Peticolas. 1975. Melting and premelting phenomenon in DNA by laser Raman scattering. *Biopolymers.* 14:247–264.

Gruenwedel, D. W. 1975. Salt effects on the denaturation of DNA. IV. A calorimetric study of the helix-coil conversion of the alternating copolymer Poly[d(A-T)]. *Biochim. Biophys. Acta.* 395:246–257.

Hinz, H. J. 1986. Thermodynamic parameters for protein-protein and protein-ligand interaction by differential scanning microcalorimetry. *Methods Enzymol.* 59–79.

Lafleur, L., J. Rice, and G. J. Thomas, Jr. 1972. Raman studies of nucleic acids. VII. Poly(A) · poly(U) and poly(G) · poly(C). *Biopolymers.* 11: 2423–2437.

Langlais, M., H. A. Tajmir-Riahi, and R. Savoie. 1990. Raman spectroscopic study of the effects of Ca^{2+}, Mg^{2+}, Zn^{2+}, and Cd^{2+} ions on calf thymus DNA: binding sites and conformational changes. *Biopolymers.* 30:743–752.

Morikawa, K., M. Tsuboi, S. Takahashi, Y. Kyogoku, Y. Mitsui, Y. Iitaka, and G. J. Thomas, Jr. 1973. The vibrational spectra and structure of poly(rA-rU) · poly(rA-rU). *Biopolymers.* 12:799–816.

Nishimura, Y., M. Tsuboi, T. Sato, and K. Akoi. 1986. Conformation-sensitive Raman lines of mononucleotides and their use in a structure analysis of polynucleotides: guanine and cytosine nucleotides. *J. Mol. Struct.* 146:123–153.

Oliver, A. L., R. M. Wartell, and R. L. Ratliff. 1977. Helix coil transitions of $d(A)_n \cdot d(T)_n$, $d(A\text{-}T)_n \cdot d(A\text{-}T)_n$, and $d(A\text{-}A\text{-}T)_n \cdot d(A\text{-}T\text{-}T)_n$. Evaluation of parameters governing DNA stability. *Biopolymers.* 16: 1115–1137.

Peticolas, W. L., W. L. Kubasek, G. A. Thomas, and M. Tsuboi. 1987. Nucleic acids. *In* Biological Applications of Raman Spectroscopy, Vol. 1. T. G. Spiro, editor. Wiley-Interscience, New York. 81–133.

Prescott, B., W. Steinmetz, and G. J. Thomas, Jr. 1984. Characterization of DNA structures by laser Raman spectroscopy. *Biopolymers.* 23: 235–256.

Puppels, G. J., C. Otto, J. Greve, M. Robert-Nicoud, D. J. Arndt-Jovin, and T. M. Jovin. 1994. Raman microspectroscopic study of low-pH-induced changes in DNA structure of polytene chromosomes. *Biochemistry.* 33:3386–3395.

Rimai, L., V. M. Maher, D. Gill, I. Salmeen, and J. J. McCormick. 1974. The temperature dependence of Raman intensities of DNA. Evidence for premelting changes and correlations with ultraviolet spectra. *Biochim. Biophys. Acta.* 361:155–165.

Small, E. W., and W. L. Peticolas. 1971. Conformational dependence of the Raman scattering intensities from polynucleotides. III. Order-disorder changes in helical structures. *Biopolymers.* 10:69–88, 1377–1416.

Stangret, J., and R. Savoie. 1992. Vibrational spectroscopic study of the interaction of metal ions with diethyl phosphate, a model for biological systems. *Can. J. Chem.* 70:2875–2883.

Strzelecka, T. E., and R. L. Rill. 1987. Solid-state 31P NMR studies of DNA liquid crystalline phases. Isotropic to cholesteric transition. *J. Am. Chem. Soc.* 109:4513–4518.

Sturtevant, J. M. 1987. Biochemical applications of differential scanning calorimetry. *Annu. Rev. Phys. Chem.* 38:463–488.

Tajmir-Riahi, H. A., M. Langlais, and R. Savoie. 1988. A laser Raman spectroscopic study of the interaction of calf-thymus DNA with Cu(II) and Pb(II) ions: metal ion binding and DNA conformational changes. *Nucleic Acids. Res.* 16:751–762.

Thomas, G. J., Jr., and J. M. Benevides. 1985. An A-helix structure for poly(dA-dT) · poly(dA-dT). *Biopolymers.* 24:1101–1105.

Thomas, G. J., Jr., J. M. Benevides, S. A. Overman, T. Ueda, K. Ushizawa, M. Saitoh, and M. Tsuboi. 1995. Polarized Raman spectroscopy of oriented fibers of *A* DNA and *B* DNA: anisotropic and isotropic local Raman tensors of base and backbone vibrations. *Biophys. J.* 68: 1073–1088.

Thomas, G. J., Jr., and K. A. Hartman. 1973. Raman studies of nucleic acids. VIII. Estimation of RNA secondary structure from Raman scattering by phosphate-group vibrations. *Biochim. Biophys. Acta.* 312: 311–322.

Thomas, G. J., Jr., G. C. Medeiros, and K. A. Hartman. 1971. The dependence of Raman scattering on the conformation of ribosomal RNA. *Biochem. Biophys. Res. Commun.* 44:587–592.

Thomas, G. J., Jr., and M. Tsuboi. 1993. Raman spectroscopy of nucleic acids and their complexes. *Adv. Biophys. Chem.* 3:1–70.

Thomas, G. J., Jr., and A. H.-J. Wang. 1988. Laser Raman spectroscopy of nucleic acids. *Nucl. Acids Mol. Biol.* 2:1–30.

Tomlinson, B. L., and W. L. Peticolas. 1970. Conformational dependence of Raman scattering intensities in polyadenylic acid. *J. Chem. Phys.* 52:2154–2156.

Wada, A., S. Yabuki, Y. Husimi, and J. G. Brahms. 1980. Fine structure in the thermal denaturation of DNA: high temperature resolution spectrophotometric studies. *CRC Crit. Rev. Biochem.* 9:87–144.

Wang, L., M. Ferrari, and V. A. Bloomfield. 1990. Large-scale preparation of mononucleosomal DNA from calf thymus for biophysical studies. *BioTechniques.* 9:24–27.